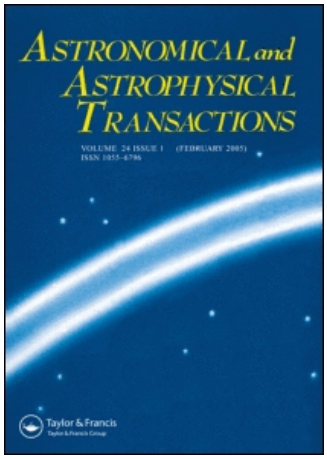

Astronomical & Astrophysical Transactions
The Journal of the Eurasian Astronomical Society
Publication details, including instructions for authors and subscription information:
http://www.informaworld.com/smpp/title~content=t713453505

Dynamics of dust grains near the Sun

L. I. Shestakova [a]; L. V. Tambovtseva [a]
[a] Fesenkov Astrophysical Institute, Almaty, Kazakhstan

Online Publication Date: 01 July 1995
To cite this Article: Shestakova, L. I. and Tambovtseva, L. V. (1995) 'Dynamics of dust grains near the Sun', Astronomical & Astrophysical Transactions, 8:1, 59 - 81
To link to this article: DOI: 10.1080/10556799508203297
URL: http://dx.doi.org/10.1080/10556799508203297

Astronomical and Astrophysical Transactions, 1995,
Vol. 8, pp. 59–81
Reprints available directly from the publisher.
Photocopying permitted by license only

DYNAMICS OF DUST GRAINS NEAR THE SUN

L. I. SHESTAKOVA and L. V. TAMBOVTSEVA

Fesenkov Astrophysical Institute, 480068, Almaty, Kazakhstan

(Received November 30, 1994)

The orbital motion of interplanetary dust grains in sublimation zone near the Sun is revised in detail for grains of obsidian, basalt, astronomical silicate and graphite. Effects of gravity, radiation pressure for a spherical source with limb darkening, and solar wind pressure on dust grains were taken into account. The influence of sputtering, thermal velocity and tangential velocity component of the solar wind particles on lifetime of the grains moving on prograde and retrograde orbits is investigated. It is obtained that β = radiation pressure/gravity is constant everywhere including the region close to the Sun.

It is shown that the temperature of submicron dust grains does not exceed 1500 K for silicate grains and 2000 K for graphite ones anywhere in solar corona. Both the dust rings observed near $9r_\odot$ and the dust free zone near $6.5r_\odot$ can be explained by basalt-like grains. These dust rings and those observed earlier near $4r_\odot$, formed by obsidian-like grains, were not found during the solar eclipse in 1991. This is possible if the bulk of the grains belong to population II (Le Sergeant D'Hendecourt and Lamy, 1980) (in this case small particles with radii $s < 0.5$ μm do not form a region of high concentration) of if dust have a cometary origin.

Dust grains with optical properties similar to astronomical silicate sublimating far from the Sun, go onto elliptic orbits and reach the Earth. These grains can be candidates for α-meteoroids) ("apex" particles) with the mass 10^{-12} g which were observed in the inner Solar System during Helios 1/2 missions.

KEY WORDS F-corona, dust grains, solar wind

1 INTRODUCTION

After reports of Peterson (1967) and MacQueen (1968) on detecting local maxima of the dust thermal emission in F-corona at the wavelengths 2.2 and 3.5 μm at the heliocentric distances 3.4, 4.0, 8.7, and 9.2 solar radii ($r_\odot$), studies appeared where model calculations had been made in order to explain these results. Kaiser's model (Kaiser, 1970) explained the existence of these maxima by two hypothetic materials: material I was responsible for the origin of the dust thermal emission at 3.4 and 8.7 $r_\odot$; material II, for that at 4.0 and 9.2 $r_\odot$. The inner maxima were explained by sublimation of "Rayleigh" particles, the outer maxima being due to sublimation of the large ones. From the modern point of view, this model is too simplified. Nevertheless, it stimulated investigations in this field.

With appearance of new data on refractive indices in a large range of wavelengths for different minerals, the Mie theory was used to calculate the emission spectra of these materials for different temperatures T_g and size s of dust grains. It became possible to obtain a temperature distribution of grains using the accurate measurements of the energy distribution in the solar spectrum. An important study of this type was published by Roser and Staude (1978). Numerical calculations of the orbital motion of dust grains in the sublimation zone near the Sun contributed significantly to the solution of this problem (Lamy, 1974a, b; Mukai *et al.*, 1974; Mukai and Yamamoto, 1979). The review by Burns *et al.* (1979) summarized the results of investigations of dust grain dynamics. These authors analyzed different aspects of the radiation pressure effect on small grains in the solar system. All papers concerned with the problem of the orbital motion of dust grains, beginning with that Belton (1966), point out that regions occur where grains stop to spiral inward and start to move outward. The concentration of grains increases in such regions. Therefore it is a natural conclusion that the regions of grain concentration have to coincide with the maxima of the thermal emission of dust grains observed in F-corona. In this case the problem of modeling turns to selection of the suitable sort of the grains, whose regions of concentration, obtained by calculation of the orbits, will coincide with the heliocentric distances where the maxima of the thermal emission were observed.

However, the situation turned out to be more complex. Later observations of the corona in infrared (IR) region (see review by Koutchmy and Lamy, 1985) showed that the maximum of the thermal emission at $4.0r_\odot$ was absent although the apparatus sensibility was sufficient for its detection. These results were reported by Mampaso *et al.* (1982) (out-of-eclipse observations using a screening disk) and Zirker (1984) (observations during the solar eclipse in 1980). During the same eclipse (Keller and Liedenberg, 1981) an IR excess at $9r_\odot$ at the wavelengths 0.7–2.2 μm and lack of any features up to 20 $r_\odot$ were registered. Further, a weak feature at $4r_\odot$ was again detected at $\lambda = 1.25$ and 1.65 μm during the eclipse in 1983 but only to the West from the Sun (Maihara *et al.*, 1985). No features at $\lambda = 2.25$ μm were detected. During the solar eclipse in 1991 no excess was found at the wavelength range from 1.2 to 2.24 μm in the distance range from 3 to 15 $r_\odot$ (Hodapp *et al.*, 1992; MacQueen *et al.*, 1992; Lamy *et al.*, 1992; Mann and MacQueen, 1993).

The observations of Lena *et al.* (1974) in the middle IR region of the spectrum at $\lambda = 8$–13 μm indicated an overall high level of intensity, significantly higher than that in the near IR region. This fact was explained by the excess of concentration of small silicate grains in F-corona.

The observations of two-dimensional picture of dust radial velocities in the elongation range from 3 to $6r_\odot$ using Fraunhofer lines near $\lambda = 5200$ Å by Shcheglov *et al.* (1987) and Shestakova (1987) revealed a boundary of the dust free zone at 6.5 $r_\odot$ in the assumption of an undisturbed outer dust region where the number density varies as $n(r) \propto n_0(r/r_\odot)^{-1.1}$. The mean grain size $\bar{s} = 0.4$ μm satisfies the observations. Classical observations of F-corona in the visible region up to large distances (Blackwell, 1955) have a good agreement with the modeling results of Ingham (1961) who suggested the mean grain size $\bar{s} = 0.3$ μm. Meanwhile, the

numerical modeling and direct space measurements of zodiacal light showed that the grain radii must be equal to 10–100 μm.

A contradiction between the observational results and those of modeling stimulated the present paper. In particular, we reconsidered the thermal balance and dynamics of the dust grains in circumsolar envelope using new, more accurate data on the energy distribution in the solar spectrum (Makarova *et al.*, 1991) and refractive indices of astronomical silicate and graphite (Drain, 1985). We also carried out detailed theoretical analysis of all components of the equation of motion and checked the influence of other weaker effects.

The orbital motion of the grains with the size $0.01 \div 1.0$ μm in the sublimation zone was calculated for graphite and silicate of four sorts: p-obsidian (poor with iron oxide), r-obsidian (rich with iron oxide), basalt and astronomical silicate (hereafter a-silicate) whose concentration zones cover a large range of distances from 2.6 to 27 $r_\odot$.

The results of calculations of the thermal balance for dust grains are given in section 2. The effect of gravitational force, radiation pressure, solar wind pressure and radiation and corpuscular drag forces was taken into account in the equation of motion (Section 3). We analyzed the accuracy of the formulae used, took into account the influence of the sphericity of the radiation source and limb darkening on dust heating and radiation pressure. The influence of nonradial motion of the solar wind on the lifetime of the dust grains moving on prograde and retrograde orbits is investigated. The effect of chaotic motion of the solar wind particles on the grain lifetime is considered. The results of calculations of the radiation pressure effect on dust grains are presented in the same section. In Section 4 we consider the orbital evolution of the dust grains depending on the number of revolutions. We investigated also the influence of the mass density and sputtering on the grain lifetime. The discussion of the results of calculations and their comparison with observational data are presented in Section 5.

2 THE TEMPERATURE OF DUST GRAINS

The main source of heating for a dust grain is absorbed solar energy which depends on the irradiance at different heliocentric distances. To consider the geometrical effects we assume the radiation to be monochromatic. Figure 1 gives a geometrical position of a grain irradiated by the spherical source. Here $r_\odot$ is solar radius, r is the distance of the grain P from the center of the Sun S, l is the distance of the grain from the arbitrary point T on the Sun's surface, θ is the angle between ST and TP directions, ψ and v are the angles at the tops S and P respectively, $\vec{e}_r$ and $\vec{e}_\varphi$ are the radial and tangential unit vectors respectively; the direction of $\vec{e}_\varphi$ coincides with the direction of the circular Keplerian motion of the grain.

The irradiance of the grain in the point P, expressed through the values measured from the Earth, is

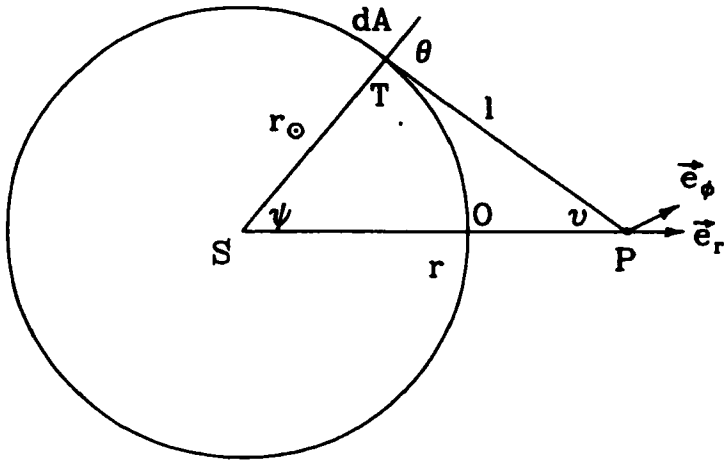

Figure 1 Geometry for calculations of irradiance and radiation pressure from spherical source.

$$E = \frac{E_\oplus \Omega}{\Omega_\oplus} - \frac{E_\oplus}{\Omega_\oplus}\left(\frac{1}{F_\lambda/I_0} - 1\right)(2\Omega - 3\Omega'), \tag{1}$$

where $E_\oplus, \Omega_\oplus$ are the irradiance and the solid angle subtended by the Sun, respectively, obtained from the Earth, $\Omega = 2\pi(1 - \sqrt{1 - r_\odot^2/r^2})$ is the solid angle subtended by the Sun from the arbitrary distance r, F_λ/I_0 is a ratio of the intensity averaged over the solar disk to that in the center of the disk. According to Baumbach (1937), the expression for Ω' for a spherical source taking into account the limb darkening is

$$\Omega' = \pi\left[1 + \frac{r^2 - r_\odot^2}{2rr_\odot}\ln\left(\frac{r - r_\odot}{r + r_\odot}\right)\right]$$

It is quite sufficient to use the first term of Eq. (1) for calculations in the region $r > 2r_\odot$ since the contribution of the second term to the total sum does not exceed 2% according to our estimations. The total energy incident on the grain is obtained by integration of Eq. (1) over all wavelengths

$$E_{\text{abs}} = \pi s^2 \frac{\Omega}{\Omega_\oplus}\int_{\lambda_1}^{\lambda_2} Q_{\text{abs}}(\lambda, s, m^*) E_\oplus(\lambda)\, d\lambda, \tag{2}$$

where $Q_{\text{abs}}(\lambda, s, m^*)$ is the efficiency factor for absorption, $m^*(\lambda) = n(\lambda) - ik(\lambda)$ is refractive index of the grain material, $E_\oplus(\lambda)$ is the energy distribution in the solar spectrum (Makarova *et al.*, 1991). Eq. (2) was used in dynamical calculations by other authors without any restrictions. In particular it is invalid in form (2) for

calculations of dynamics of quartz whose zone of sublimation occurs at $r < 2r_\odot$ (Lamy, 1974b).

In order to check the validity of integration limits ($\lambda_1 = 0.15$ μm, $\lambda_2 = 50$ μm), the integral in Eq. (2) was taken for different regions of the spectrum and a contribution of each region to the total integral has been determined. Our estimations show that contribution into heating the grains does not always correspond to the energy distribution in the solar spectrum, especially for p-obsidian which has the lowest absorption coefficient $k(\lambda)$ around the maximum of the solar radiation. Heating a-silicate and graphite grains correlates best of all with the energy distribution. The integration limits chosen are quite sufficient for all materials of interest in the range of sizes from 0.01 to 1 μm. Moreover, one can use a narrower range $\lambda_1 - \lambda_2 = 0.20$–$20$ μm for a-silicate and 0.20–5 μm for graphite.

The energy loss due to sublimation (Lamy, 1974b) and heating due to collisions with solar wind particles (Mukai and Schwehm, 1981) are found to be unimportant in total thermal balance of grains considered. Therefore, we used a simplified equation of the thermal balance to determine the distribution of the grain temperature with the distance in the form

$$E_{\rm abs} = E_{\rm rad}, \tag{3}$$

where $E_{\rm abs}$ is given by Eq. (2) and $E_{\rm rad} = 4\pi s^2 \int_{\lambda_1}^{\lambda_2} Q_{\rm abs}(\lambda, s, m^*) B(\lambda, T_g)\, d\lambda$ is the energy lost by a grain on the radiation; $B(\lambda, T_g)$ is Plank's function.

Check of validity of integration limits for $E_{\rm rad}$ shows that all irradiated energy concentrates in the wavelength region from 1 to 30 μm for all silicate grains (T_g = 500–1200 K) and from 0.6 to 20 μm for graphite grains since their characteristic temperatures are systematically higher (T_g = 1100–1800 K).

The efficiency factor $Q_{\rm abs}(\lambda, s, m^*)$ was computed using the Mie theory. The refractive indices for obsidian and basalt were taken from Lamy (1978) for λ = 0.15–0.30 μm and Pollack *et al.* (1973) for λ = 0.30–50 μm. The refractive indices for a-silicate and graphite were taken from Drain (1985) for all wavelength range λ = 0.15–50 μm.

The temperature distribution on silicate grains is illustrated by Figure 2. The grain temperature T_g is given as a function of $r_\odot/r$ for the grains with radii $s_{\rm min}$ = 0.01, $s_{\rm max}$ = 1.0 μm and one intermediate grain size. Figure 3 gives the dependence $T_g(s)$ for all silicate grains at the fixed distances from the Sun. All of them, except r-obsidian, show a temperature maximum for a certain intermediate size s = 0.2–0.3 μm. It is seen from Figure 2 that the grains just of these radii have a temperature distribution deviating most of all from the boundary ($s_{\rm min}, s_{\rm max}$) curves. The radial temperature law, close to the blackbody one $T_g \propto T_0 r^{-0.5}$, is obtained only for a-silicate and graphite grains with s = 1.0 μm. For submicron graphite grains the power index is close to –0.35, for a-silicate grains it is about –0.53; the universal law for obsidian and basalt grains was not found in the whole range of temperatures. For T_g = 1000–1300 K the power index varies from –0.76 (basalt, s = 1.0 μm) to –1.5 (obsidian, s = 0.01 μm).

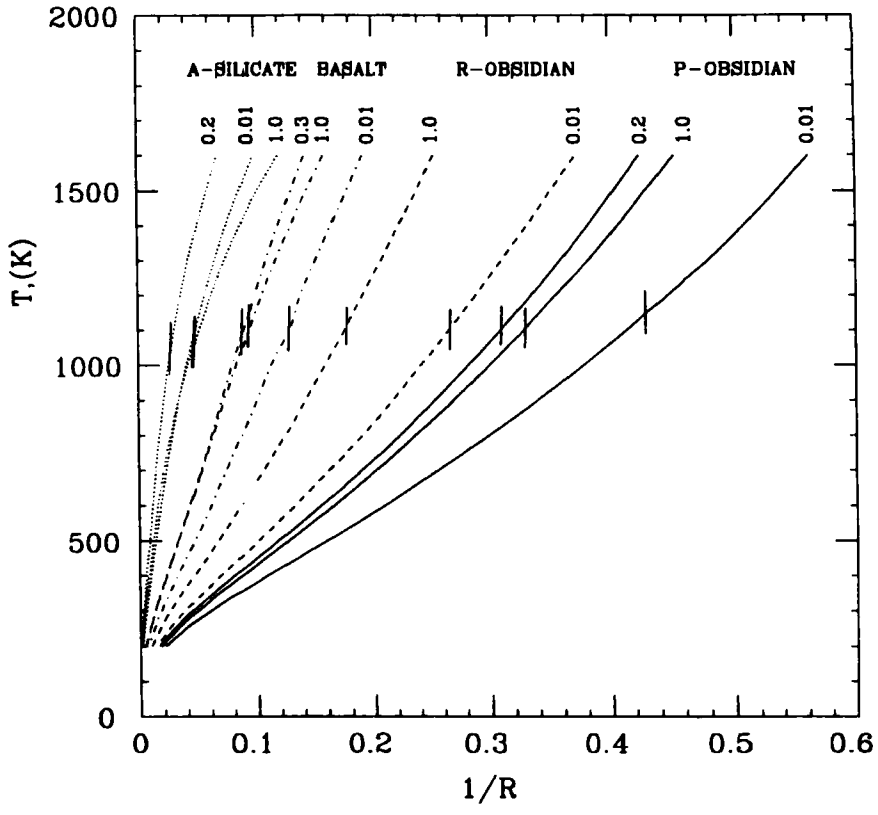

Figure 2 Grain temperature as a function of inverse heliocentric distance. Solid dashed, dashed-dotted and dotted curves denote the temperature of p-obsidian, r-obsidian, basal and a-silicate respectively. The numbers indicate grain radii in units of μm. The vertical scales bars boundaries of the influence of two processes: sublimation and sputtering.

Thus, using a certain temperature law $T_g(r)$ for dust grains in the solar system limits chemical composition and range of grain sizes.

3 EQUATION OF MOTION

Taking into account main forces acting on a dust grain, gravitational force F_g radiation pressure F_r and solar wind pressure F_w, one can write down the equation of motion as follows

$$m\ddot{\vec{r}} = -F_g\vec{e}_r + F_r\left[\left(1-\frac{\dot{r}}{c}\right)\vec{e}_r - \frac{\vec{V}_k}{c}\right] + \frac{F_w(\vec{V}_w-\vec{V}_k)}{|\vec{V}_w-\vec{V}_k|}, \qquad (4)$$

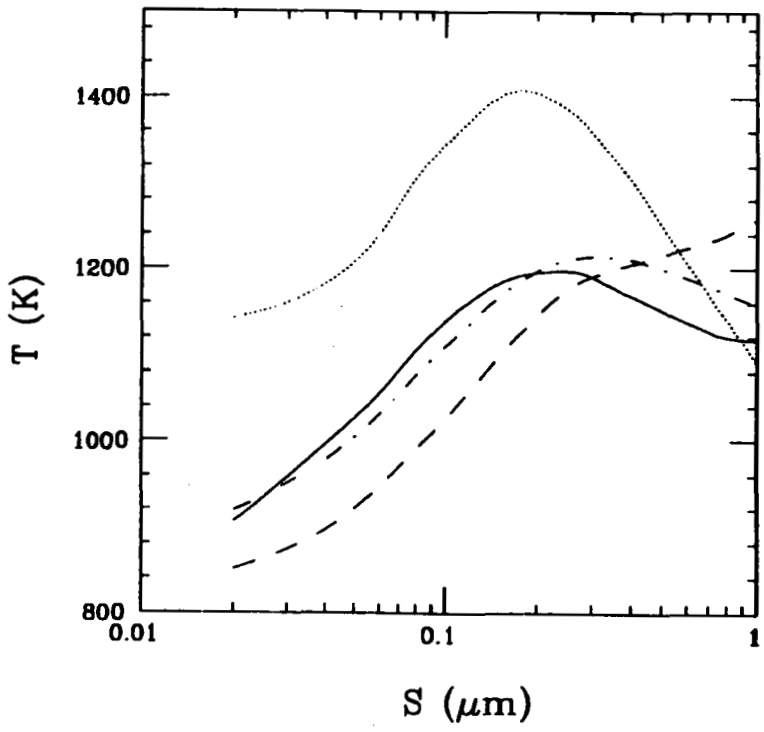

Figure 3 Size dependence of grain temperature at the fixed distances from the he Sun: $3r_\odot$ for p-obsidian (solid line) $5r_\odot$ for r-obsidian (dashed line) $10r_\odot$ for basalt (dashed-dotted line), $20r_\odot$ for a-silicate (dotted line).

where F_g, F_r and F_w are modules of the forces mentioned above; c, $\vec{V}_k$ and $\vec{V}_w$ are velocities of light, grain orbital motion and the solar wind respectively. The second term of Eq. (4) is the same as in paper of Burns *et al.* (1979), the third one is taken from the paper of Baines *et al.* (1965).

3.1 The effect of radiation pressure on the dust grain

The radiation pressure F_r, for a spherical source taking into account limb darkening can be derived in non-relativistic approach quite correctly using the same method as for irradiance. A grain in the point P (Figure 1) experiences the effect of forces from all elementary areas dA on the solar surface. Contrary to the case of irradiance consideration, here we have to take into account the angle ν, determined by the direction of the radiation pressure action. The radial component of the radiation pressure from the area dA is

$$dF = \pi s^2 Q_{\rm pr}(\lambda, s, m^*) \frac{dE}{c} \cos \nu \qquad (5)$$

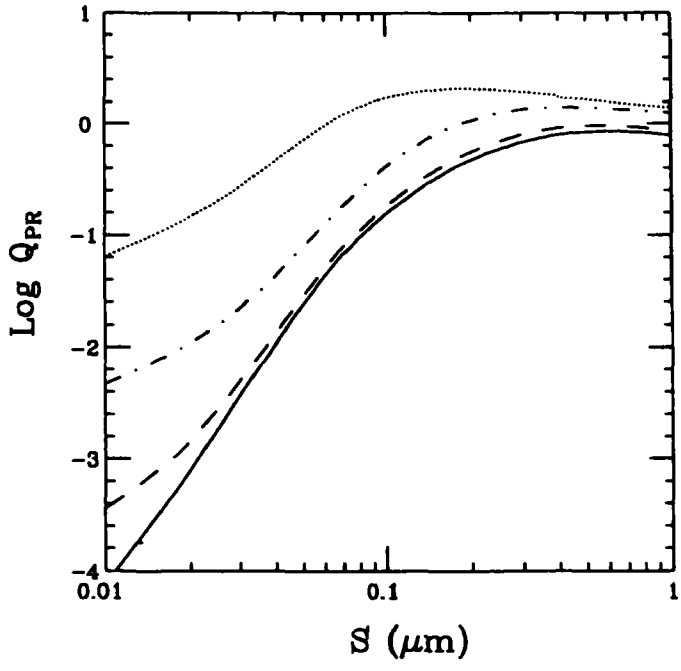

Figure 4 Dependence of the radiation pressure efficiencies on the grain size for different materials. Solid line refers to p and r-obsidian, dashed line to basalt, dashed-dotted line to a-silicate, and dotted line to graphite.

where $Q_{\rm pr}(\lambda, s, m^*)$ is the efficiency factor for radiative pressure computed using the Mie theory (further, $Q_{\rm pr}(\lambda, s)$ for simplicity). As the result, the expression for radiation pressure has a trivial form

$$F_r = \frac{\pi s^2}{c}\frac{r_0^2}{r^2}\int_{\lambda_1}^{\lambda_2} Q_{\rm pr}(\lambda, s) E_\oplus(\lambda)\, d\lambda \tag{6}$$

where $r_0 = 1$ AU. Note that mechanical substitution of the parameter Ω from the expression for irradiance (Eq. 2) into the expression for the force (Eq. 6) is incorrect for representation of F_r from a spherical source. It follows from Eq. 6 that $\beta = F_r/F_g$ =*const everywhere including the region near the Sun*. We will use the second term of Eq. 4 corrected for sphericity according to conclusion of Guess (1962):

$$F_r\left[\vec{e}_r - \frac{r\dot{\phi}}{c}\left(1 + \frac{1}{2}\frac{r_\odot^2}{r^2}\right)\vec{e}_\phi\right]. \tag{7}$$

The introduced correction $(\frac{1}{2}r_\odot^2/r^2)$ suffices the accuracy of calculations in the region $r \geq 2r_\odot$. We neglect the relativistic terms of the order $\dot{r}/c$. Special analysis

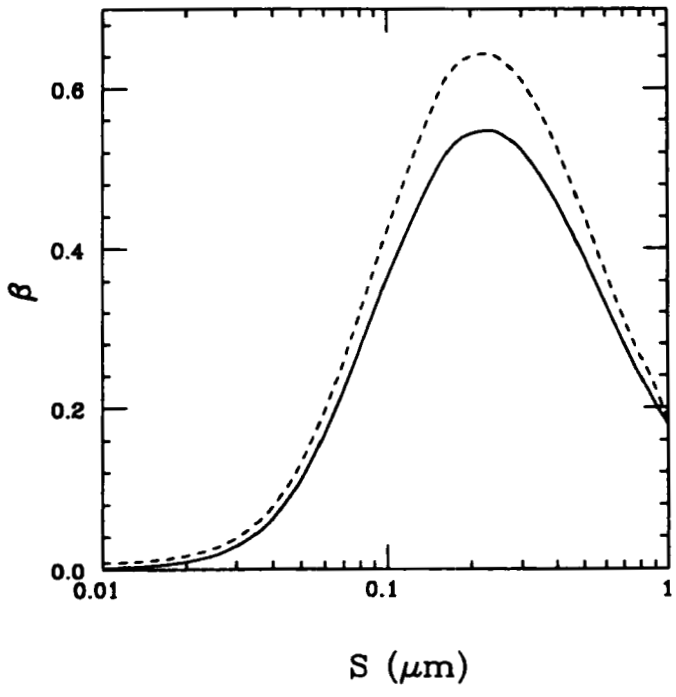

Figure 5 The ratio of radiation pressure to gravitational force $\beta = F_r/F_g$ as a function of grain size for p and r-obsidian (solid line) and basalt (dashed line).

shows that all remarks made for the integration limits for the integral in Eq. 2 are valid for that in Eq. 6.

The parameter $Q_{\rm pr}(s)$ which is important for dynamical calculations, can be determined as mean weighted over the solar spectrum:

$$Q_{\rm pr} = \frac{\int\limits_0^\infty Q_{\rm pr}(\lambda, s) E_\oplus(\lambda)\, d\lambda}{\int\limits_0^\infty E_\oplus(\lambda)\, d\lambda} = \frac{I}{E}, \tag{8}$$

where I is the integral in Eq. 6, $E_0 = 0.1369 \times 10^7$ erg cm^{-2} c^{-1} is the solar constant according to precise data of Makarova *et al.* (1991). In this case

$$\beta = \frac{3 Q_{\rm pr}(s) L_\odot}{16 \pi c M \delta s} = \frac{5.78 \times 10^{-5} Q_{\rm pr}(s)}{\delta s}, \tag{9}$$

where $L_\odot$ is the luminosity of the Sun, $M = GM_\odot$ is the gravitational constant of the Sun, $M_\odot$ is its mass and G is the universal gravitational constant. The mass density δ and the radius of a grain are given in g cm^{-3} and cm respectively. Eq. 9 is very similar to analogical equation in the paper by Burns *et al.* (1979). The results of calculations of $Q_{\rm pr}(s)$ and β are presented in Figures 4, 5, and 6.

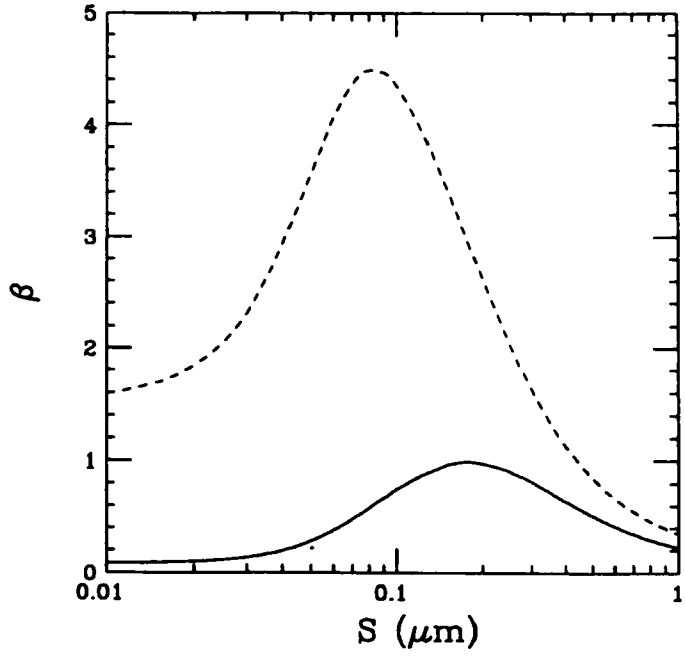

Figure 6 Same as Figure 5., for a-silicate (solid line) and graphite (dashed line).

3.2 The solar wind effect

The dust particle moving through a gas is exposed to the action of the resistance force which has the following form (Baines *et al*, 1965):

$$F_w = \pi s^3 \sum_i m_i n_i U_i^2 C_i, \tag{10}$$

where

$$C_i = \frac{1}{\sqrt{\pi}} \left(\frac{1}{S_i} + 12 S_i^3 \right) e^{-S_i^2} + erf(S_i) \left(1 + \frac{1}{S_i^2} - \frac{1}{4 S_i^4} \right) + \frac{\sqrt{\pi}}{3 S_i} \sqrt{\frac{T_g m_g}{T_i m_i}} Y_i.$$

Here m_i, n_i, T_i are the mass, the number density and the temperature of the gas particles of the given species, $U_i = |\vec{V}_i - \vec{V}_k|$ is the relative velocity of the motion of the dust and gas particles. Parameter $S_i = U / \left(\frac{2kT_i}{m_i} \right)^{1/2}$ is the velocity ratio of the directed grain motion to the thermal one of the gas, m_g is the mass of the dust grain, Y_i is the sputtering yield which depends on the sort of either projectile or target particle. The third term in the expression for C_i differs from that in paper by Baines *et al.* (1965) because we deal with the sputtering due to impacts of solar wind particles instead of diffuse scattering of the incident ones. We assume that

Table 1. The influence of the wind thermal motion on the lifetime of p-obsidian dust grains

$s(\mu m)$	1.0	0.5	0.3	0.2	0.02
t_c/t	0.997	0.972	0.999	0.991	0.978

molecules leave a spherical dust grain with velocities obey the Maxwell law with the temperature T_g. Our result differs from that of Mukai and Yamamoto (1982) whose parameter m_g/m_i is a linear multiplier (Eq. 3 in the cited paper). This means that they overestimated increase of the resistance force F_w due to sputtering by a factor of $\sqrt{m_g/m_i}$. Our estimations give a negligible contribution of sputtering processes to the effect of solar wind pressure on the grain (less than 5%).

We can consider the solar wind as consisting of protons and α-particles (Svalgaard, 1977). For these sort of particles, the equality of velocities (not energies) both for directed and chaotic motion takes place. Thus, one can assume that $U_p = U_\alpha = |\vec{V}_w - \vec{V}_k|, s_p = s_\alpha, C_p = C_\alpha$, where indices p and α refer to protons and α-particles respectively. Since $\sum_i m_i n_i = m_p n_p \mu_w$, where $\mu_w = 1 + \mu_\alpha \chi_\alpha$ is the mean molecular weight of the solar wind particles, χ_α is the abundance of α-particles, then Eq.10 is significantly simplified:

$$F_w = \pi s^2 m_p n_p \mu_w U^2 C = \frac{s^2 U^2 \dot{M}_\odot C}{4r^2 V_{wr}}, \tag{11}$$

where $\dot{M}_\odot$ is the mass loss rate of the Sun, V_{wr} is the radial velocity of the solar wind, $C = 1/\sqrt{\pi}(1/s + 1/2s^3)\exp -s^2 + erf(s)(1 + 1/s^2 - 1/4s^4)$ is a parameter taking into account the thermal motion of the wind particles. In the approximation of large velocities of the directed motion, $s \to \infty$ and $C = 1$. The maximal deviation from this approximation is expected for grains which reach the nearest distance from the Sun and have mass densities smaller than standard ones. In order to check the effect of the thermal motion of the wind particles on dust grain dynamics we carried out the numerical calculations of evolution of p-obsidian grains with low mass loss density $\delta = 1.5$ g cm^{-3}. The results are presented in Table 1. Here t is the lifetime of the grains till total sublimation or till departure from the stationary orbit when $C = 1$, T_c is the same, but with account of thermal velocities of the solar wind particles at $T_p = 0.7 \times 10^6$ K. The initial distance is $3r_\odot$.

It is clear from Table 1 that the thermal motion of the solar wind particles is negligible both for grains leaving the Solar System ($s > 0.4$ μm) and for those falling on the Sun ($s \leq 0.4$ μm). Thus, we can assume in the following that $C = 1$. In this case the ratio of forces F_w/F_g has a simple form

$$\beta' = \frac{3\dot{M}_\odot U^2}{16\pi M \delta s V_{wr}} = \frac{5.71 \times 10^{-16}}{\delta s} \frac{U^2}{V_{wr}}, \tag{12}$$

where δ is in g cm^{-3}, s is in cm, U and V_{wr} are in cm s^{-1}. For large distances one can assume $U = V_{wr} = 400$ km s^{-1}, then $\beta' = 2.28 \times 10^{-8}/\delta s$.

Table 2. The effect of non-radial motion of the solar wind on the grain lifetime

grain material	$s(\mu m)$	1.0	0.1	0.02
p-obsidian	t_{retr}/t_{pr}	0.94	0.93	0.93
$r_0 = 3r_\odot$	t_{pr}/t	1.031	1.038	1.011
basalt	t_{retr}/t_{pr}	0.97	0.83	0.75
$r_0 = 10r_\odot$	t_{pr}/t	1.037	1.111	1.150

When expanding the wind velocity on unit vectors we obtain $\vec{V}_w = V_w \cos\theta\vec{e}_r + V_w \sin\theta\vec{e}_\phi$, where θ is the angle between the direction of the wind motion and the unit vector. According to Svalgaard (1977) this angle is 1°.5 at the Earth's orbit. The radial velocity component in Eqs. 11 and 12 is $V_{wr} = V_w \cos\theta$. In the region of the wind coronation the angular velocities of the Sun ($\omega_\odot$) and the wind ($V_w \sin\theta/r$) coincide. For prograde orbital motion third term in Eq. 4 will be

$$\frac{F_w}{U}\left[(V_w\cos\theta - \dot{r})\vec{e}_r + (V_w\sin\theta - r\dot{\phi})\vec{e}_\phi\right]. \tag{13}$$

After all transformations Eq. 4 has a form convenient for numerical calculations in the circumsolar region $r \geq 2r_\odot$:

$$\begin{aligned} \ddot{r} - r\dot{\phi}^2 &= -\frac{M}{r^2}\left[1 - \beta - \beta'\frac{V_w\cos\theta - \dot{r}}{U}\right], \\ \frac{d}{dt}(r^2\dot{\phi}) &= -\alpha\left(1 + \frac{1}{2}\frac{r_\odot^2}{r^2}\right)\dot{\phi} - \alpha'(\dot{\phi} - \omega), \end{aligned} \tag{14}$$

where $\alpha = \beta M/c$, $\alpha' = \beta' M/U$, $\omega = V_w \sin\theta/r$ is the angular velocity of the wind which changes its sign when we deal with retrograde motion. The second equation of the system (14) allows to calculate the angular momentum loss of the grain depending on drag forces. The ratio of Poynting–Robertson drag force due to the solar wind to that due to radiation is $J = \alpha'/\alpha$ in our notation. It is easy to find this ratio for grains with large sizes (10–100 μm) in a zodiacal cloud, $J_0 = M_\odot c^2/L_\odot = 0.30$.

We present in Table 2 the results of calculations of prograde and retrograde motion for p-obsidian and basalt grains in assumption that the coronation zone reaches $12r_\odot$ (Priest, 1982). Here t is the lifetime of the grain till the total sublimation in the case of radial solar wind, t_{pr} and t_{retr}, same for cases of prograde and retrograde motion respectively when $\omega = \omega_\odot$, r_0 is the initial distance. Calculations are made for grains with a standard mass density $\delta = 2.5$ g cm^{-3}.

It is seen from Table 2 that non-radial motion of the solar wind does not influence significantly the grain lifetime. The main results of the present paper are obtained in assumption of the radial solar wind ($\omega = 0$, $\theta = 0$) and large relative velocities ($C = 1$).

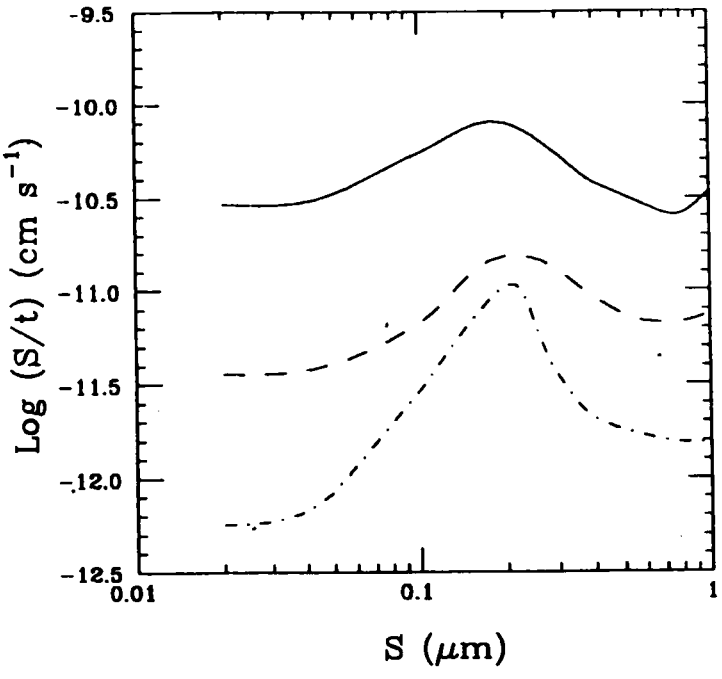

Figure 7 The averaged rate of full sublimation as a function of initial grain size.

4 THE NUMERICAL RESULTS

To calculate the grain orbits, we made the following assumptions:

i) Spherical grains of p, r-obsidian, basalt, a-silicate, and graphite stars with the circular orbital velocity near the region of intensive sublimation at the initial distances r_0 equal to 3.0, 5.0–6.0, 10, 20–28, and 6.0 $r_\odot$ respectively.

ii) The standard mass densities are 3.2 g cm^{-3} for a-silicate, 2.5 g cm^{-3} for other silicate grains, and 2.3 g cm^{-3} for graphite. Molecular weight is $\mu_g = 67$ for silicate and $\mu_g = 12$ for graphite.

iii) The solar wind velocity is determined on the base of Parker's model (Parker, 1963); solar wind is assumed to be isothermal with the mass loss rate $\dot{M}_\odot = 2 \times 10^{-14} M_\odot$ yr^{-1} and the velocity at the Earth's orbits equals to 400 km s^{-1}.

iv) Grains sublimate isotropically, reactive forces are absent and thermal conduction processes run very rapidly. The sublimation rate was computed according to Lamy (1974a, b) for silicate and to Mukai and Yamamoto (1979) for graphite.

v) We neglect the planets' influence and collisions between grains. Grains are electrically neutral. Figure 7 illustrates dependence of $\log(s/t)$ on s. Here s is the initial size of the grain and t is the lifetime of the grain until total evaporation. It is seen from the figure that the grains with radii about 0.2 μm have the maximal mean sublimation rate. The short lifetime of these grains is explained by dynami-

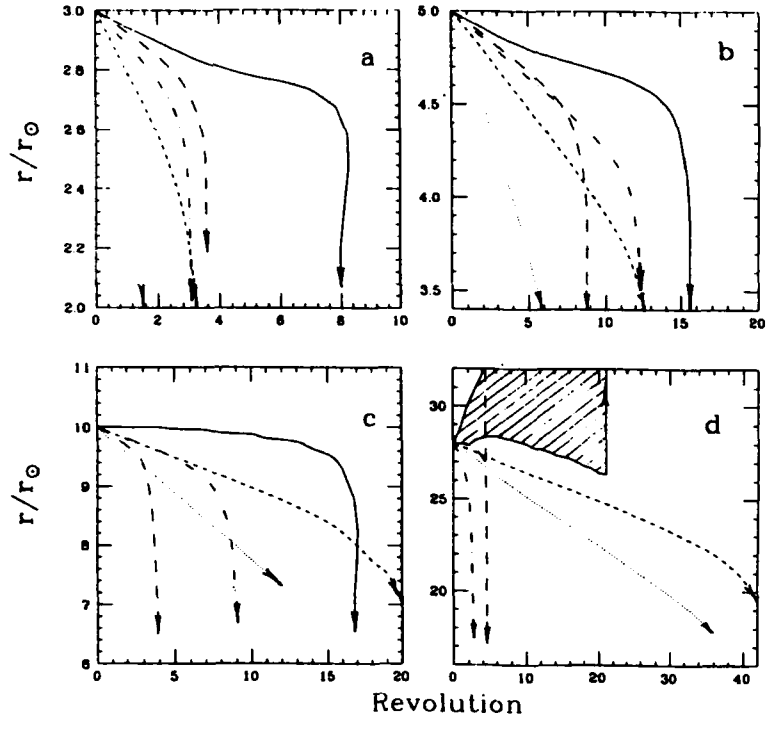

Figure 8 The orbital evolution of silicate grains near the Sun for (a), p-obsidian; (b), r-obsidian; (c), basalt and (d), a-silicate. Small particles. The solid line refers to $s_0 = 0.3$ μm, the dashed line to $s_0 = 0.2$ μm, the dashed-dotted line to $s_0 = 0.1$ μm, the short dashed line to $s_0 = 0.05$ μm, and the dotted line to $s_0 = 0.02$ μm. The lower boundary of the shaded region is perihelion of the orbit, the upper one is aphelion.

cal reasons, namely, by their transition onto elliptic orbits with a small perihelion distance. The orbital evolution of the small grains ($s \leq 0.3$ μm) and the large ones ($s > 0.3$ μm) is shown in Figures 8 and 9.

4.1 Small grains

The lifetime of small grains (number of revolutions) is determined, mainly, by two causes: the velocity of motion towards the Sun under the influence of Poynting–Robertson law ($\sim 1/rs$) and the sublimation rate which depends on the grain temperature. It is seen from Figure 8 that the curves $r(n)$ for obsidian grains whose sublimation zones are near the Sun line up according to Poynting–Robertson law, i.e., the curve slopes increase with decrease of s. For basalt and a-silicate grains sublimating farther from the Sun such a sequence of the curve slopes does not occur since the grains come to the sublimation zone at once when starting from r_0. Figure 7 shows that the maximal averaged sublimation rate corresponds to the silicate grains with $s \sim 0.2$ μm, therefore the lifetime of the grains with $s = 0.1$–0.2 μm,

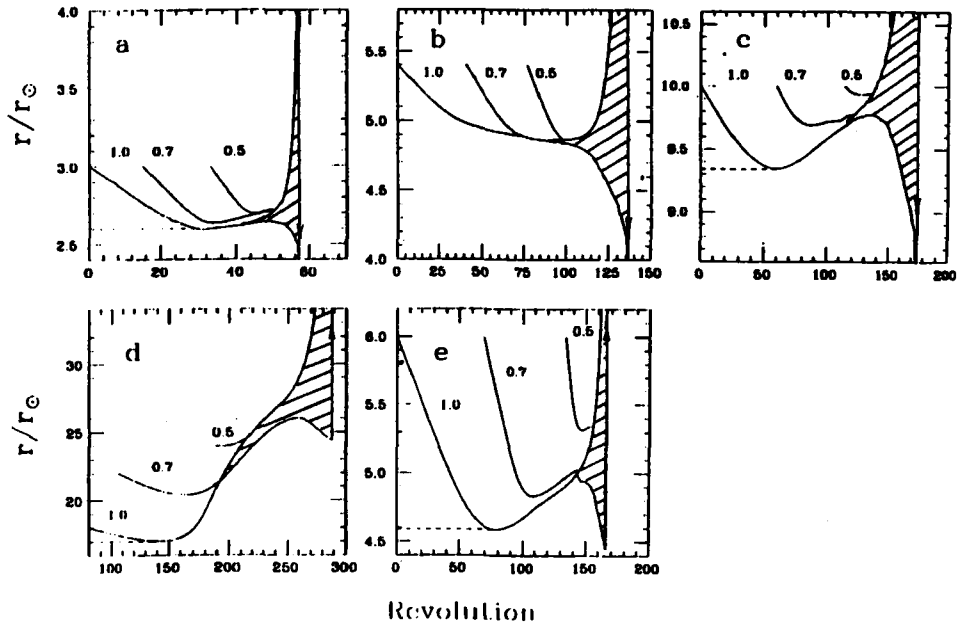

Figure 9 Same as Figure 8; (e) graphite. Large grains. Numbers are initial grain sizes in μm. The distances the grains undergo intense sublimation (r_{min}) are marked with the dashed line.

entering the sublimation zone immediately, is less than that of both larger and smaller grains. Figure 8c, d clearly demonstrates this. Situation for a-silicate is different: the grains with $s \geq 0.3$ μm leave the Solar System and the grains with $s = 0.2$ μm go onto highly elongated orbits before falling onto the Sun. In such cases we give a dependence $q(n)$ (e.g., Figure 8d or Figure 9a–e for large grains) where q is perihelion distance. The region between perihelion and aphelion of the orbit is shaded.

4.2 Large grains

The orbital evolution scenario for the larger grains is more complex. As in the case of small grains, the initial slopes of the curves $r(n)$ near the start distance are distributed according to Poynting–Robertson law. In the region of sublimation an abrupt deceleration of grain infall occurs. Having approached the minimal distance (r_{min} in Figure 9 a, c, d), the grains begin to move away from the Sun and in the final stage of evaporation, on reaching the size of 0.5–0.3 μm, go onto highly elongated elliptic orbits (shaded in Figure 9). Then, on reaching the size of 0.3–0.2 μm, the grains fall on the Sun practically immediately (during the time which is less than the Keplerian period). R-obsidian grains do not show the increase of perihelion because of different behavior of $T(s)$ (Figure 3), but a plateau where $r \approx const$ is expressed clearer. The orbital evolution of the p-obsidian grains with the initial size

1.0 μm (Figure 9a) practically coincides with that in Burns *et al.* (1979). Lamy (1974 a, b) made a conclusion that there were no grains with $s = 0.2$ μm in corona. We conclude that this is valid only for the sublimation region of the grains.

It is seen from Figure 9 that concentration of the grains with given sizes has to grow near the plateau. Since the position of $r_{\min}$ depends on the grain size, the increase of concentration will be most significant for the grains of radius s_1, i.e., the lower limit of the grain distribution to the power law $n(s) = n_0 s^{-\nu}$, where $s_1 < s < s_2$ (s_2 is the upper limit of this distribution). Our calculations show that the region of high concentration (the dust ring around the Sun) forms if $s_1 \geq 0.5$ μm. Smaller grains fall on the Sun without formation of a high concentration region.

When considering dynamics of the grains with $s > 0.5$ μm one has to pay attention to the following:

1) Since all grains with initial radius $s > 0.5$ μm come to the region shaded in Figure 9 on a certain stage of their evolution, the enrichment of the corona by the grains with very narrow size range $s = 0.5$–0.3 μm due to the transition of the latter onto high elliptic orbits takes place.

2) The grains whose sublimation occurs far from the Sun (a-silicate) cannot form a region of high concentration due to the strong broadening of this region (in Figure 9d the distance r changes from 17 to $27 r_\odot$ for $s = 1$ μm). Besides that, in the process of the "oscillation", the grains with $s = 0.4$–0.3 μm reach the Earth's orbit and can be observed near the aphelion of their orbits like "apex" particles with a small angular momentum. These are so-called α-meteoroids observed in the inner Solar System during Helios 1/2 missions. For $\delta = 2.5$ g cm^{-3} this range of sizes corresponds to the mass $m_g = 10^{-12}$ g, more probable for apex particles. The a-silicate grains of smaller sizes become β-meteoroids.

4.3 Sublimation of large grains

The sublimation rate of silicate (Lamy, 1974b) for $T_g = 1200$–1300 K can be described by the simple linear formula

$$\log |\delta \frac{ds}{dt}| = -30.871 + 1.583 \times 10^{-2} T_g. \tag{15}$$

Since the orbits of the grains with the initial sizes $s \geq 0.5$ μm become highly eccentric, we calculated the mean orbital sublimation rate over one Keplerian period. The results in the form of the dependence of $\log |\overline{ds/dt}|$ on the number of revolutions n are presented in Figure 10. For all sorts of grains the mean sublimation rate becomes stabilized and a plateau forms where $\overline{ds/dt} \approx const$. These values and corresponding grain temperatures are given in Table 3. The sublimation rate on the plateau is different for different materials. We suggest an empirical formula connecting this parameter with the perihelion distance q for silicate:

$$|\delta \frac{\overline{ds}}{dt}| = 6.75 \times 10^{-10} q^{-2.5}, \tag{16}$$

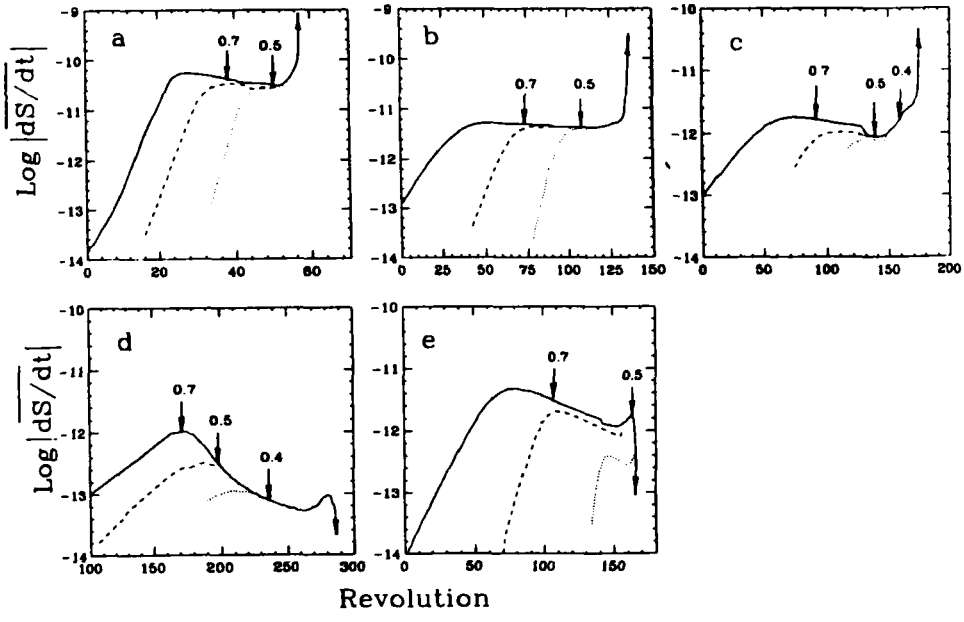

Figure 10 Dependence of the averaged sublimation rate on the revolution number for (a), p-obsidian; (b), r-obsidian; (c), basalt; (d), a-silicate and (e), graphite. Large grains. Arrows mark the mean size for the grain with the initial size 1 μm.

where q is given in the units of the solar radius and $|\overline{ds/dt}|$ is in cm s^{-1}. In Figure 10 the intermediate sizes are marked for the grain with an initial size 1 μm. It appears that the graphite and a-silicate grains become β-meteoroids having sublimated to 0.5 μm and 0.3 μm respectively. Other silicate grains fall on the Sun when sublimating to 0.2 μm.

It should be noted that the temperature $T_{\max}$ at which the grains evaporate completely are significantly lower than melting temperatures for the material considered. The silicate grains melt at $T = 1980$ K (Pollack *et al.*, 1973), the graphite ones at $T = 3925$ K (Wickramasinghe and Guillaume, 1965). Our calculations show that the uppermost temperatures at the final stage of sublimation do not exceed

Table 3. The temperature characteristics at the plateau and on the boundary of complete sublimation

	p-obsidian	*r-obsidian*	*basalt*	*a-silicate*	*graphite*
$q(r_\odot)$	2.6	4.9	9.8	27	4.9
$\overline{T_g(K)}$	1315	1255	1215	1150	1950
$\log\|\overline{ds/dt}\|$	-10.5	-11.35	-12.05	-13.25	-11.60
$r_s(r_\odot)$	1.9	2.9	6.0	14	4.5
$T_{\max}$(K)	1470	1435	1410	1390	2036

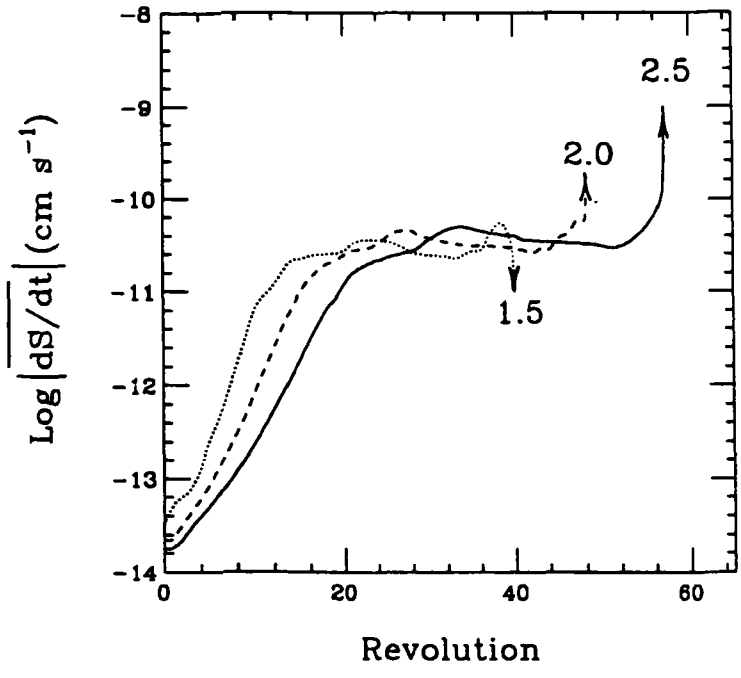

Figure 11 Dependence of the average sublimation rate on the revolution number for p-obsidian grains with initial size 1 μm. δ = 2.5 g cm^{-3} (solid line), δ = 2.0 g cm^{-3} (dashed line), and δ = 1.5 g cm^{-3} (dotted line).

1500 K for silicate grains and 2050 K for graphite ones. Unfortunately, this circumstance is not always taken into account in calculations of the thermal emission in F-corona. For example, Mann (1992)) assumed non-realistic maximal dust grain temperatures equal to 2300 K at $4r_{\odot}$.

Table 3 presents the values of the maximal grain temperatures $T_{\max}$ which the grains have on the boundary of the complete sublimation r_s. It is seen from Table 3 that the regions of possible concentration of the grains (q) and the boundary of the complete sublimation r are spatially separated.

4.4 The influence of mass density on grain lifetime

We carried out the calculations of orbital evolution for p-obsidian and basalt grains with mass density less than the standard one Figure 11 presents the results of these calculations as a dependence of the mean sublimation rate on the number of revolution for p-obsidian grains with the initial size 1.0 μm and mass densities equal to 2.5, 2.0 and 1.5 g cm^{-3}. Figure 11 shows that the position of the plateau is about the same for these grains and the revolution number (not lifetime) decreases with decrease of δ. We present the ratio of the lifetimes $t_{1.5}/t_{2.5}$ for p-obsidian and basalt and ratio $t_{2.0}/t_{2.5}$ for p-obsidian (the lower indices denote the values of mass

Table 4. The ratio of the lifetime of grains with different mass densities

material	$s(\mu m)$	*1.0*	*0.5*	*0.3*	*0.2*	*0.1*	*0.05*	*0.02*	$\delta/2.5$
p-obsidian	$t_{2.0}/t_{2.5}$	1.047	1.058	1.036	0.860	0.828	0.800	0.820	0.8
$r_0 = 3r_\odot$	$t_{1.5}/t_{2.5}$	1.176	1.114	1.733	0.600	0.650	0.620	0.620	0.6
basalt	$t_{1.5}/t_{2.5}$	0.747	1.639	0.035	0.083	0.407	0.500	0.570	0.6
$r_0 = 10R_\odot$									

Table 5. The influence of sputtering on the lifetime of p-obsidian grains with the standard mass density

$s(\mu m)$	0.5	0.4	0.3	0.2	0.1	0.05	0.02
t_{sp}/t	0.996	1.000	1.000	0.990	0.950	0.970	0.960

density). The last column in the table gives the ratio of the mass density to the standard one.

Finally the grains with $\delta = 2.0$ g cm^{-3} fall on the Sun and the grains with $\delta = 1.5$ g cm^{-3} leave the Solar System. The lifetime of the latter can grow compared to the standard case due to the high ellipticity of their orbits but can also decrease due to their rapid departure from the stationary orbit. Only the grains with a small initial size $s_0 < 0.1$ μm fall on the Sun according to the law close to the Poynting–Robertson one and their lifetime is proportional to δ (see Table 4). The lifetime of large grains (especially near the boundary of their "destiny change" (fall or escape) can strongly change depending on different weaker effects: sputtering, presence of the tangential velocity component of the solar wind, etc.

4.5 Sputtering

We can express, referring to Whipple (1955), the change of the radius of the grain moving on an eccentric orbit due to sputtering in the following form:

$$\frac{ds}{dt} = -\frac{\mu_g \dot{M}_\odot Y}{16\pi\mu_w \delta a^{3/2} p^{1/2}}, \tag{17}$$

where $a, e, p = a(1-e^2)$ are the semimajor axis eccentricity and the parameter of the orbit respectively. The sputtering yield Y is assumed to be equal to 0.048 according to Drain and Salpeter (1979) for the velocity of the collisions of dust grains with wind particles $U \approx 200$ km s^{-1} in the circumsolar region and the mean fraction of α-particles in the solar wind equal to 0.05. The influence of this process on the grain lifetime in the sublimation zone at normal (standard) mass density is negligible as it is seen from Table 5. Here t_{sp} is the lifetime of a grain when sputtering is taken into account; start distance $r_0 = 3r_\odot$.

At small mass densities ($\delta = 1.5$ g cm^{-3}), especially near the boundary "fall-escape", the effect of sputtering can be significant. For example, for a "falling"

p-obsidian grain with $s_0 = 0.4$ μm, the lifetime decreases by more than a factor of 10 compared to the standard case, while for a "leaving" grain with $s_0 = 0.5$ μm and a "falling" one with $s_0 = 0.3$ μm the lifetime increases by $\sim$10%.

During the long evolution of dust grains in the Solar System beyond the sublimation zone, the main cause of the decrease of the grain size (besides mutual collisions) is the sputtering process. In Figure 2 the vertical lines mark the areas of the influence of the two processes: nearer the Sun sublimation dominates, further, sputtering becomes important.

5 DISCUSSION AND CONCLUSIONS

Only few among the numerous observations of F-corona in the visible and IR regions of the spectrum contain real information about the region nearest to the Sun. These are the observations of the corona in IR and the observations of the radial velocities of the circumsolar dust.

Unfortunately, IR observations of the corona on July 11, 1991 were restricted to the region $r \leq 15 r_\odot$ where no excess of thermal radiation was found (Lamy *et al.*, 1992; Hodapp *et al.*, 1992). The results of calculations obtained for basalt show the best fit to earlier observations of F-corona in IR (MacQueen, 1968; Keller and Liedenberg, 1981) when an IR excess has been detected near $9 r_\odot$, and they are in agreement with the observations of the radial velocities of the dust grains in F-corona (Shcheglov *et al.*, 1987; Shestakova, 1987). The observations of the thermal emission of F-corona at 8–13 μm (Léna *et al.*, 1974) show that a rise of its intensity nearest to the Sun corresponds to the distance range 3–5 $r_\odot$. This coincides with the location of r-obsidian grains from our modeling which gives a boundary of the complete sublimation at 3 $r_\odot$ and the region of the density enhancement at 4.8 $r_\odot$ for such grains with $s \geq 0.5$ μm. According to Léna *et al.* (1974) the thermal emission has a minimum at 5–6 $r_\odot$ and has the rise of intensity at 6.5 $r_\odot$. As it follows from the modeling, this second feature can be explained by basalt-like dust grains whose boundary of complete sublimation is close to 6 $r_\odot$ and the region of the concentration of these grains with $s \geq 0.5$ μm is at about 9.5 $r_\odot$. Thus, our calculations of dynamics of r-obsidian and basalt grains are in agreement with observations by Léna *et al.* (1974).

We summarize the theoretical results and compare them with those of observations in Table 6. It should be mentioned that besides coincidence of the computed concentration zone (q) and the boundary of complete sublimation (r_s) of the basalt grains with the corresponding observational data, the mean grain sizes $\bar{s}$ and the lower limit of the grain size s_1 in the dust grain distribution are nearly the same as observational ones. The grain sizes obtained from the calculations are typical of all sorts of silicate grains. The location of the inner thermal emission excess at 4,0–4.2 $r_\odot$ can be caused by material intermediate between p and r-obsidian as it is follows from previous calculations by Lamy (1974a, b) and Mukai and Yamamoto (1979). Irregularity of the appearance of this excess, in particular, its absence during the solar eclipse in 1991, can indicate that either this matter has cometary

Table 6. Comparison of the computed orbital parameters with observational data

Parameters	*Calculations*	*Observations*	*References*
$q(r)$, the distance of high concentration	9.2–9.8 basalt	8.7–9.2 9.0	MaqQueen (1968) Keller and Liedenberg (1981)
$r_s/r_\odot$, the boundary of complete evaporation	6.0 basalt	6.5±0.5	Shcheglov *et al.* (1987) Shestakova (1987)
$\bar{s}$, the mean radius of grains	0.5–0.3 all materials	0.4	Shestakova (1987)
s_1 (μm) the lower limit of grain radius	0.2 all materials	0.2	Shestakova (1988)

origin or it belongs mainly to the population II for which $s_2 \leq 1$–1.5 μm. A small decrease of the upper limit s_2 leads to disappearance of the concentration zone of dust grains.

Considering orbital evolution of a-silicate grains, whose sublimation zone is relatively far from the Sun, gives a new observational aspect for sublimating grains. In particular, in the range of sizes from 0.5 to 0.3 μm ($m_g \approx 10^{-12}$ g) they can be observed in the inner Solar System near aphelions of their orbits as α-meteoroid, i.e., as "apex" particles with small angular momentum. Such particles were detected during Helios 1/2 missions. High ellipticity of the orbits occurring due to sublimation processes is favorable for the grains to leave the circumsolar region. It can also lead to the grains' departure from stationary orbits and to their turning into β-meteoroids.

The main conclusions of this paper are as follows:

Silicate grains with the size range 0.01–0.2 μm fall onto the Sun without forming regions of high concentration; their lifetimes are directly proportional to their mass densities as it follows from the Poynting–Robertson law.

For small silicate grains with $s < 0.1$ μm the drag force due to the solar wind is stronger than that due to radiation. For grains of a zodiacal cloud ($s = 10$–100 μm), the ratio of this forces is $\dot{M}c^2/L = 0.3$.

Silicate and graphite grains with $s \geq 0.5$ μm from the regions of high concentration independently of the final results: fall on the Sun or leaving the Solar System.

The outer regions of the corona are enriched with the dust grains with $s = 0.5$–0.3 μm due to transition of the grains onto the highly elliptic orbits.

The mean temperatures of silicate grains with sizes from 0.01 to 1 μm in the regions of concentration are in the range from 1150 K (a-silicate) to 1315 K (p-obsidian).

The maximal temperatures of silicate grains do not exceed 1500 K on the boundary of the complete sublimation.

The dust rings observed near $9r_\odot$ and the dust free zone near $6.5r_\odot$ can be explained by basalt-like grains. The irregularity of appearance of these rings as well

of those near $4r_\odot$, formed by obsidian-like grains, can be understood if the dust grains have a cometary origin or belong to population II.

The grains sublimated far from the Sun (a-silicate) can be observed near aphelions of their orbits as α-meteoroids with the mas $m_g = 10^{-12}$ g.

A-silicate grains with $m_g \approx 10^{-13}$ g and graphite grains with $m < 10^{-12}$ g become β-meteoroids.

References

Baines, M. J., Williams, I. P., and Asebiomo, A. S. (1965) *MN* **130**, 63.
Baumbach, S. (1937) *Astron. Nachr* **263**, 121.
Belton, M. J. S. (1966) *Sci* **151**, 35.
Blackwell, D. E. (1955) *MN* **115**, 629.
Burns, J. A., Lamy, P. L., and Soter, S. (1979) *Icarus* **40**, 1.
Drain, B. T. (1985) *Ap. J. S.* **57**, 587.
Drain, B. T. and Salpeter, E. E. (1979) *Ap. J.* **231**, 77.
Guess, A. W. (1962) *Ap. J.* **135**, 855.
Hodapp, K.-W., MacQueen, R. M., and Hall, D. N. B. (1992a) *Nat.* **335**, 707.
Hodapp, K.-W., Rayner, J., and Irwin, E. (1992b) *PAS. J.* **104**, 441.
Ingham, M. F. (1961) *MN* **122**, 157.
Kaiser, C. B. (1970) *Ap. J.* **159**, 77.
Keller, C. F. and Liedenberg, D. (1981) *Los Alamos Science*, LANL **2**, 4.
Koutchmy, S. and Lamy, P. L. (1985) In *Properties and interactions of Interplanetary Dust*, Giese R. H., Lamy P. L. (eds.), Reidel, Dordrecht, p. 63.
Lamy, P. L. (1974a) *Astron. Astrophys.* **33**, 191.
Lamy, P. L. (1974b) *Astron. Astrophys.* **35**, 197.
Lamy, P. L. (1978) *Icarus* **34**, 68.
Lamy, P. L., Kuhn, J. R., Lin, H., Koutchmy, S., and Smartt, R. N. (1992) *Sci* **257**, 1377.
Le Sergeant D'Hendecourt, L. B. and Lamy, P. L. (1980) *Icarus* **43**, 350.
Léna, P., Viala, Y., Hall, D., and Soufflot, A. (1974) *Astron. Astrophys.* **37**, 81.
MacQueen, R. M. (1968) *Ap. J.* **154**, 1059.
Mann, I. (1992) *Astron. Astrophys.* **261**, 329.
Mann, I. and MacQueen, R. M. (1993) *Astron. Astrophys.* **275**, 293.
Maihara, T., Mizutani, K., and Hiromoto, N., *et al.* (1985) In *Properties and Interactions of Interplanetary Dust*, Giese R. H., Lamy P. L. (eds), Reidel, Dordrecht, p. 55.
Makarova, E. A., Kharitonov, A. V., and Kazachevskaya T. V. (1991) *Solar radiation flux*, Nauka, Moscow (in Russian).
Mampaso, A., Sanchez, M. C., and Buitrago, J. (1982) In *Sun and Planetary System*, Fricke W., Tedeki G. (eds.), Reidel, Dordrecht, p. 257.
Mukai, T., Yamamoto, T., Hasegawa, A., Fujiwara, A., and Koike, C. (1974) *PAS. J.* **26**, 445.
Mukai, T. and Schwehm, G. (1981) *Astron. Astrophys.* **95**, 373.
Mukai, T. and Yamamoto, T. (1979) *PAS. J.* **31**, 585.
Mukai, T. and Yamamoto, T. (1982) *Astron. Astrophys.* **107**, 97.
Parker, E. (1963) *Interplanetary Dynamical Processes*, Interscience, New York.
Peterson, A. W. (1967) *Ap. J.* **148**, L37.
Pollack, J. B., Toon, O. B., and Khare, B. N. (1973) *Icarus* **19**, 372.
Priest, E. R. (1982) *Solar magnetohydrodynamics*, Reidel, Dordrecht.
Roser, S. and Staude, H. J. (1978) *Astron. Astrophys.* **67**, 381.
Shcheglov, P. V., Shestakova, L. I., and Ajmanov A. K. (1987) *Astron. Astrophys.* **173**, 388.
Shestakova, L. I. (1987) *Astron. Astrophys.* **175**, 289.
Shestakova, L. I. (1988) Ph. D. Thesis, Moscow University.
Svalgaard, L. (1977) In *Illustrated Glossary for Solar and Solar-Terrestrial Physics*, Bruzek A., Durrant C. J. (eds), Reidel, Dordrecht, p. 149.

Whipple, F. L. (1955) *Ap. J.* 121, 750.
Wickramasinghe, N. C. and Guillaume, C. (1965) *Nature* **207**, 366.
Zirker, J. B. (1984) *Total Eclipse of the Sun*, VNR Company Publ., New York, p. 210.